Tenth International Conference on Computational Fluid Dynamics (ICCFD10), Barcelona, Spain, July 9-13, 2018

ICCFD10-xxxx

Dynamic Mode Decomposition of Hypersonic Boundary-layer Transition on Blunt Cone

Xinliang Li[*,**], Changping Yu[*] and Fulin Tong[*,***]
Corresponding author: lixl@imech.ac.cn

[*] LHD, Institute of Mechanics, Chinese Academy of Sciences, Beijing, China
[**] School of Engineering Science, University of Chinese Academy of Sciences, Beijing, China
[***] Computational Aerodynamics Institute of China Aerodynamics Research and Development Center, Mianyang, China.

Abstract: Direct numerical simulation (DNS) of hypersonic boundary layer transition over a 7^0 half-cone-angle blunt cone at the zero angle of attack is performed. The transition is triggered by the disturbance waves induced by the wall blowing and suction. The data of wall skin friction coefficient is analyzed by dynamic mode decomposition (DMD) to clarify the dynamical relevant mechanism in transitional process. It is found that a linear superposition of low-frequency modes and second modes accurately reconstructs the structural change of wall skin friction during the transition, suggesting a possible physical mechanism for the evolution of disturbance waves.

Keywords: Direct numerical simulation, Hypersonic, Transition, Dynamic mode decomposition.

1 Introduction

Blunt cones are typical leading shape of hypersonic vehicles, and Laminar-turbulent transition of hypersonic flows over blunt cones is a hot-topic in recent researches. The transition has a significant impact on the aerodynamic heating and skin friction. For example, the surface heat rating and drag are dramatically increased due to the onset of the boundary layer transition. Owing to the obvious importance, extensive numerical researches have paid much attention on this problem in the past decades. The transition in a cone boundary layer at Mach number 3.5 is studied by Mayer *et al*. [1] to investigate the linear and weakly non-linear development of wave packet, where the transition was initiated by a wave packet. They found that the oblique breakdown might be the strongest nonlinear transition mechanism. Li *et al*. [2] systematically studied the effect of attack angle on hypersonic boundary layer transition over blunt cones. It was found that the delayed transition was caused by the suppression of the second mode's growth rates. The analysis of band-pass filter suggested that the very low frequency disturbance waves were found to be related with the large-scale nonlinear perturbations. Sivasubramanian *et al*. [3] numerically investigated the boundary layer transition on a sharp cone at Mach number 6. The controlled transitions are studied by a set of high resolution simulation to investigate the nonlinear stages of transition and the final breakdown to turbulence. The second-mode fundamental resonance or breakdowns were deemed to be a dominating mechanism responsible for the hypersonic boundary layer transition on cone. In the present work, the DNS data is analyzed using Dynamic mode decomposition to make a contribution towards further understanding of hypersonic transition over a blunt cone.

2 DNS setup

Three dimensional conservative compressible Navier-Stokes equations in cylindrical coordinates are selected as the governing equations, which are non-dimensionalized by the inflow parameters and head radius of blunt cone. More details are referred to Li et al. [2]. The working medium is perfect air. Hence, the ideal gas law is applicative and the viscosity is evaluated by the Sutherland law. The inviscid flux terms are discretized using a modified weighted essentially non-oscillatory (WENO) scheme [4] and the standard Steger-Warming splitting method. To minimize numerical dissipation and optimize the bandwidth properties, optimal weights with symmetric stencil are used in the linear part of WENO method, which is well suited for the DNS of hypersonic transitional boundary layer. The viscous flux terms are calculated using the classical eight-order central difference scheme and the time integration is performed by the explicit three-order Runge-Kutta algorithm.

In this simulation, the radius of nose tip is 1mm. The attack angle is zero and the Mach number is 6. The free stream statics temperature T_∞ and wall temperature T_w are given as 74.0 K and 294 K, respectively. The Reynolds number based on the nose radius is 10,000. A two-step procedure is applied in the simulation. Firstly, 2D laminar computation including the entire blunt cone geometry and the bow shock is performed using high-order finite difference method. Then, three-dimensional DNS of boundary-layer transition is conducted, where the computational domain locates inside the bow shock. The domain in the axial direction extends form z=70 to z=1300. The height in the wall normal direction is about 1.5δ to 10δ, corresponding to the start and end axial locations, respectively, where the boundary layer thickness δ is taken at z=1000. The domain in the azimuthal direction is a 30 degree range. The computational domain is discretized by 2000×100 ×200 (axial × wall normal × circumference) nodes. The grids in the axial and azimuthal direction are spaced equally, where the nodes in the wall-normal direction are clustered near the wall. Based on the boundary layer parameter at z=1000, the grid resolution in wall units is Δz^+=20.5, Δr_w^+=1.0, $r\Delta\theta^+$=6.7, comparable with the numerical results of Li *et al*. [2].

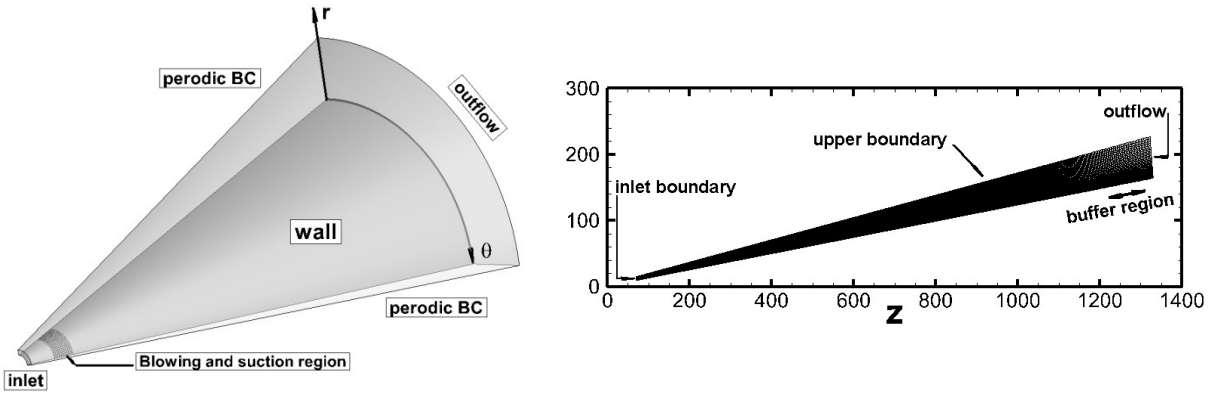

Figure 1: Illustration of computational domain and grid.

The computational domain and grid are shown in Fig.1, where boundary conditions are also imposed. In the inlet and upper boundary, dirichlet boundary conditions are applied using the steady laminar profiles of the 2D laminar steady calculation. A non-reflecting boundary with a buffer region with gradually coarsen grids is used at the outflow boundary to eliminate the reflected disturbance waves entering the domain. Periodic boundary conditions are imposed in the azimuthal direction. The wall is treated by the no-slip and isothermal boundary conditions. As suggested by Li *et al*. [2], the wall disturbances are forced within the blowing and suction region to trigger the boundary layer transition, ranging from z=90 to z=100, where the random weak disturbances with the amplitude of 0.005 are enforced on the wall as the wall-normal velocity.

3 Results and Discussions

3.1 Instantaneous and mean flow field

Fig.2 shows the coherent vortex structures in the transitional boundary layer using the Q criterion [5]. It is clear that the regular 2D vortexes occurred in the near wall region are predominant at the early stage of transition. However, the large-scale hairpin-like vortices are obviously visible in the outer region of boundary layer when the flow breaks down to turbulence. It is interesting to find that the legs of hairpin vortex are much more elongated in the streamwise direction, in contrast to the supersonic turbulent boundary layer.

Fig.3 shows the contours of instantaneous and time-averaged wall skin friction coefficient. At z< 650, little variations in the azimuthal direction are found and the distribution is characterized by the quasi-two dimensional structures, which are associated with the rope like waves induced by the second mode waves. In the range of 650<z<750, the structural modulation is obviously observed and followed by typical axial streaky pattern at z>750. The streamwise distribution of time and azimuthal direction averaged wall skin friction coefficient is plotted in Fig.4, together with the theoretical results which are calculated using the Karman-Schoenherr and Blasius formulation. Here, the red and blue colored dashed lines denote the maximum and minimum time-averaged wall skin friction in the azimuthal direction. At z<600, the skin friction agrees well with the laminar solution, then a rapid increase from the laminar profile to the turbulent curve is present in the range of 600 < z < 800, indicating that the transition is onset. It is clear that an overshoot is present in the later region of transition. At z>800, the skin friction gradually attains the turbulent theoretical solutions, suggesting the boundary layer is approaching the turbulent state.

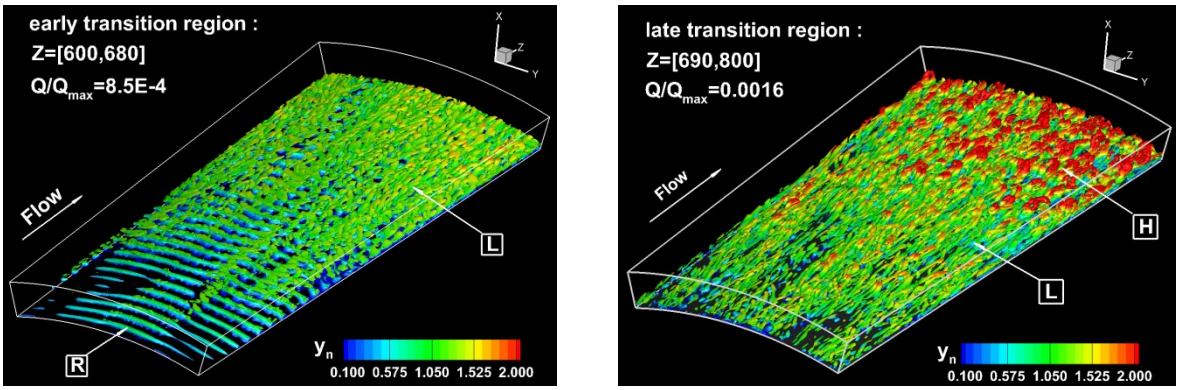

Figure 2: Coherent vortex structures in the transitional boundary layer.

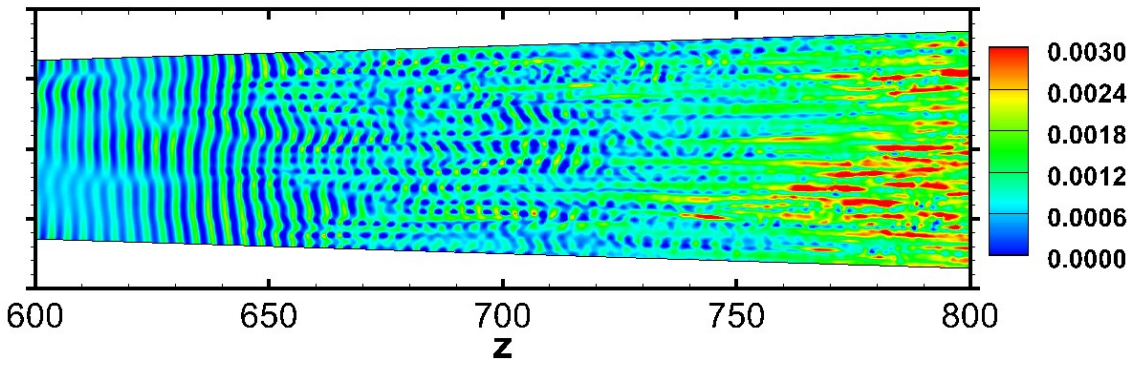

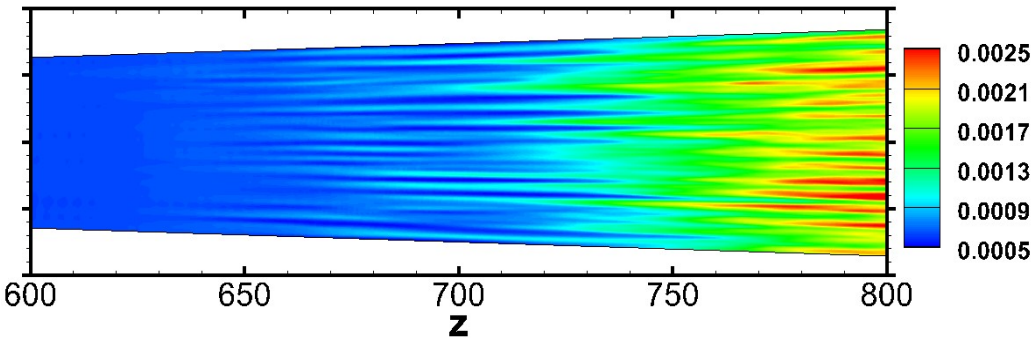

Figure 3: Contours of instantaneous (top) and mean (bottom) wall skin friction coefficient.

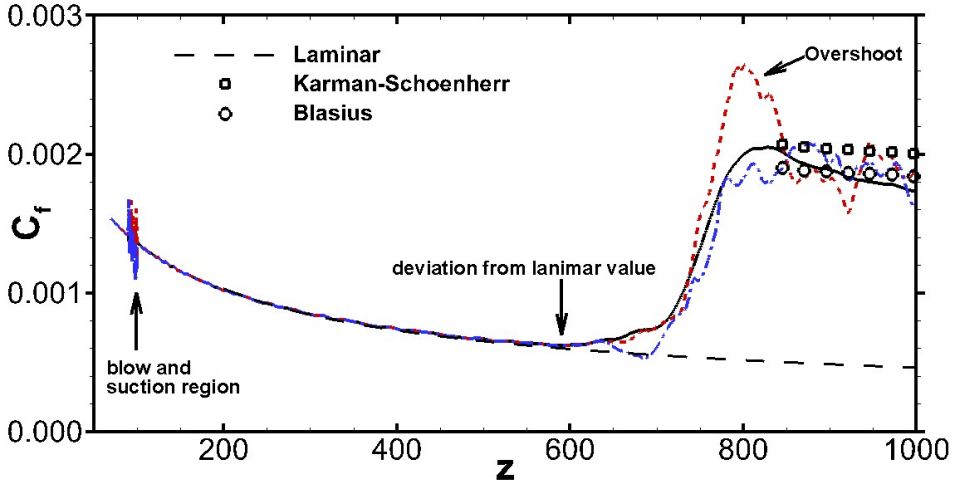

Figure 4: Distribution of wall skin friction coefficient.

3.2 Dynamic mode decomposition

In this section, dynamic mode decomposition is performed to investigate the dynamical relevant modes in the transition process. The basic steps of DMD-algorithm are outlined briefly [6]. Firstly, a snapshot sequence [V_1, V_2, V_3, ...,V_N] is formed by the instantaneous flow fields which are sampled at a constant time step, where *N* denotes the total number of snapshots. Singular value decomposition is applied to solver the low-order matrix approximating the full matrix of linear operator between the instantaneous flow fields. Then, modal frequency and growth rate are calculated by the image and real part of the low-order matrix's eigenvalues, respectively. Furthermore, the DMD modes are constructed by the eigenvectors of the low-order matrix. According to Jovanovic *et al.* [7], the sparsity-promoting DMD algorithm (DMDSP) is used to select the dynamical modes that have greatly influence on the essential features of transitional flow fields. To capture the important dynamics related with the structural changes as shown in Fig.3, DMD analysis is applied to the DNS data of instantaneous wall skin friction coefficient. The streamwise range of DMD domain is from z=550mm to z=800mm, covering both the linear and non-linear stage of transition evolution. The spanwise range extends to the edge of computational domain. The constant sampling time is about 0.00028 mill-seconds and the total number of snapshot is 400. Therefore, the corresponding frequency resolution of DMD analysis is from 9 KHz to 1783 KHz.

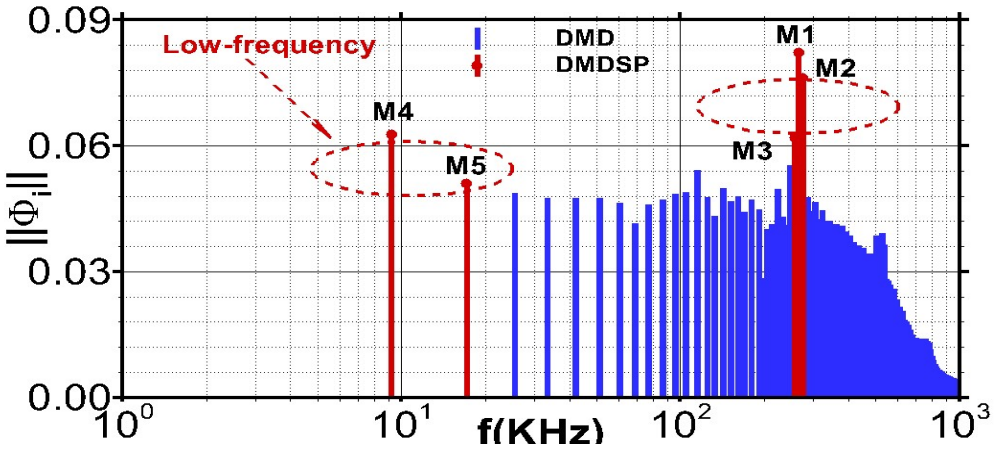

Figure 5: DMD spectrum.

Fig.5 shows the DMD spectrum, where the dependence of modal energy $\|\Phi_i\|$ on the frequency $\boldsymbol{f}$ is present. The subsets of relevant dynamical modes which are selected by the DMDSP algorithm with performance loss of 14% are denoted with the red color. Here, the norm of modes is applied as the modal energy and the performance loss is defined as $\%\Pi = 100\sqrt{J(\alpha)/J(0)}$, where α represents the amplitude of modes and $\boldsymbol{J}$ represents the objective function. More details can be found in Ref. [7]. Clearly, the DMD spectrum is broadband and the DMDSP modes are sorted into two distinct subsets according to the value of frequencies. In particular, the frequencies of modes M1-M3 are centered about 256 KHz, in good agreement with the dominated frequency of second modes in the spectral analysis of wall pressure fluctuations. However, the modes M4 and M5 are concentrated around very low frequency, about 10 KHz and 20 KHz, respectively. It is suggested that the very low frequency modes are dynamically relevant and also provide significant contribution to the transition process.

The spatial structures of dynamic modes M1-M5 are shown in Fig.6, respectively, where the real parts of different modes are compared. As is apparent in Fig.6 (a-f), the modes M1-M3 exhibit a similar behavior. For example, the structures are negligible in the early stage of transition for z< 550, where the computed skin friction coefficient coincides with the laminar solution. Moreover, the real part exhibits a rapid increase for 550<z<700, corresponding to the region of transition onset. Note that the associated shape is approximately quasi two-dimensional, consistent with the distribution of skin friction. It decreases dramatically in the later stage of transition for z >700. Accordingly, the regular 2D structures are also destroyed badly and no similar results are found clearly downstream. However, the pattern of modes M4 and M5 are utterly different. It is found that these low-frequency modes are characterized by the large-scale streaky structures, only observed in the later region of transition. Moreover, the scale of these streaky structures increases quickly after z>700, where the corresponding structures of modes M1-M3 represent the opposite behavior.

Fig.7 shows contours of the reconstructed instantaneous and time-averaged skin friction based on the dynamical modes M1-M5 and mean solution, respectively. It is interesting to find that a similar structural change of wall skin friction distribution as shown in Fig.3 is obtained. Furthermore, Fig.8 quantitatively compared the reconstructed wall skin friction with the raw DNS data. Apparently, the agreement is satisfactory through the entire transitional region, suggesting that the modes M1-M5 are essentially dynamical relevant during the dynamic process of transition. However, there is still some difference between the original DNS and reconstructed results. The main reason to account for this discrepancy might be that the computed skin friction distribution is an integration of all disturbance waves with broadband frequency spectrum. However, the reconstructed results are based on the two kinds of characteristic frequency, about $\boldsymbol{f}$=256 KHz and $\boldsymbol{f}$=10 KHz, respectively. According to above analysis, it is hypothesized that the structural change of instantaneous skin friction distribution can be described as a transformation process between modes M1-M3 and modes M4-M5.

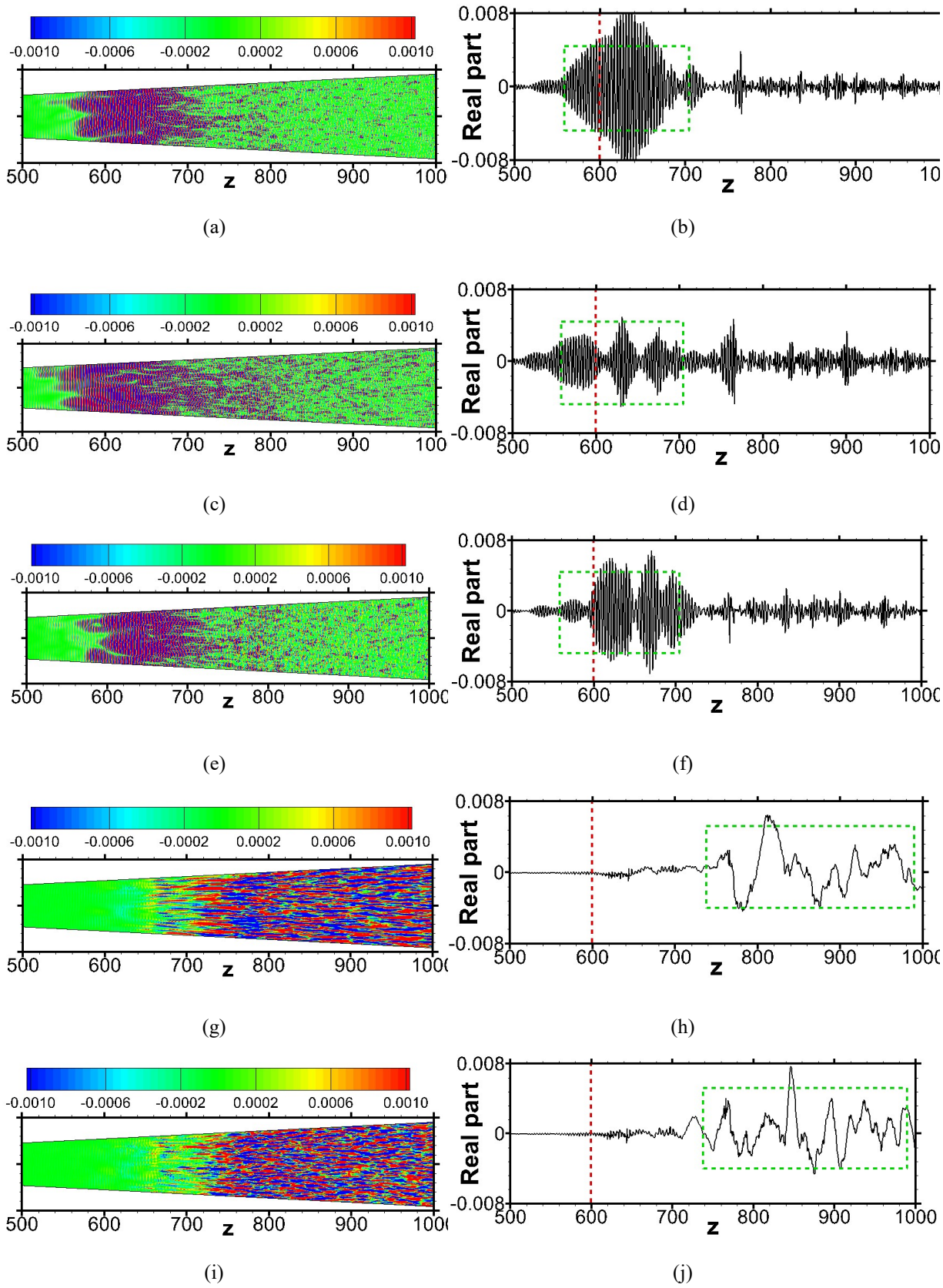

Figure 6: Real part of DMDSP modes: (a, b) M1, (c, d) M2, (e, f) M3, (g, h) M4 and (i, j) M5.

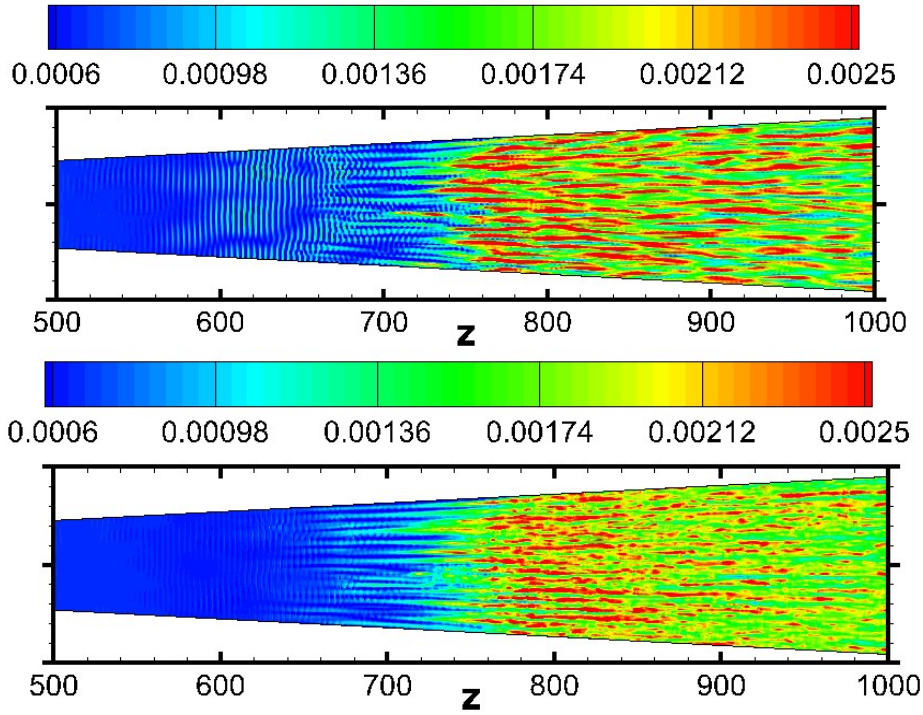

Figure 8: Contours of the reconstructed instantaneous (top) and mean (bottom) wall skin friction coefficient based on modes M1-M5.

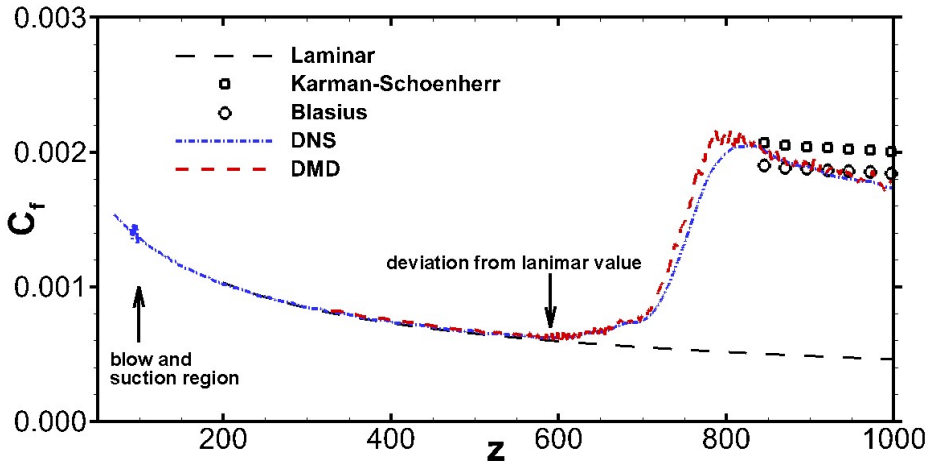

Figure 7: Distribution of the reconstructed wall skin friction coefficient based on modes M1-M5.

4 Conclusions

Direct numerical simulation of hypersonic boundary layer transition on a 7^0 half-cone-angle blunt cone is performed to improve the understanding of transition mechanism. A bandwidth-optimized WENO scheme with symmetry stencil is applied to discretize the inviscid fluxes and the eighth order central difference is used for the viscous terms. To trigger transition to turbulence, the random weak perturbations are induced into boundary layer through the blowing and suction disturbances on the wall.

Analysis of coherent vortex structures indicates that the start of transition is populated with 2D vortex in the near wall region, where the nonlinear stage of transition is characterized by hairpin vortex structures with elongated vortex legs. Visualization of instantaneous skin friction coefficient

clearly shows that the regular 2D pattern in the azimuthal direction gradually breakdowns to the typical streamwise streaky structures during the transition process. According to the DMD analysis, the structural change of skin friction in the transitional boundary layer is accurately approximated by the low frequency modes and the second modes, suggesting that the low frequency disturbances also play an important role in the breakdown to turbulence.

References

[1] C.S.J. Mayer, A.C. Laible and H.F. Fasel. Numerical Investigation of Wave Packets in a Mach 3.5 Cone Boundary Layer. AIAA J., 49(1):67-85, 2011.

[2] X.L. Li, D.X. Fu and Y.W. Ma. Direct Numerical Simulation of Hypersonic Boundary Layer Transition over a Blunt Cone. AIAA J., 46(11):2899-2911, 2008.

[3] J. Sivasubramanian and H.F. Fasel. Direct Numerical Simulation of Transition in a Sharp Cone Boundary Layer at Mach 6: Fundamental Breakdown. J. Fluid Mech, 768:175-281, 2015.

[4] M.P. Martin, E.M. Taylor, M. Wu, and V.G. Weirs. A Bandwidth-Optimized WENO Scheme for the Effective Direct Numerical Simulation of Compressible Turbulence. J. Comp. Phys, 220:270-289, 2006.

[5] J.C.R. Hunt, A.A. Wray and P. Moin. Eddies, Streams, and convergence zones in turbulent flows. AIAA J., 49(7):1336-1353, 2011.

[6] P.J. Schmid. Dynamic Mode Decomposition of Numerical and Experimental Data. J. Fluid Mech, 656:5-28, 2010.

[7] M.R. Jovanovic, P.J. Schmid and J.W. Nichols. Sparsity-Promoting Dynamic Mode Decomposition. Phys. Fluids, 26:024103, 2014.